On the soft X–ray spectra of γ–loud blazars

Andrea Comastri
Osservatorio Astronomico di Bologna

Giovanni Fossati
Scuola Internazionale Superiore di Studi Avanzati, Trieste

Gabriele Ghisellini
Osservatorio Astronomico di Merate

and

Silvano Molendi
Istituto di Fisica Cosmica e Tecnologie Relative del CNR, Milano

ABSTRACT

ROSAT observations of a large sample of bright γ–ray (E $>$ 100 MeV) blazars are presented. Results of a detailed spectral analysis in the soft $\sim$ 0.1–2.0 keV energy range are discussed in relation to the overall energy distribution with particular emphasis on the relation between X–ray and γ–ray properties. A significant anti–correlation between X–ray and γ–ray spectral shapes of flat radio spectrum quasars (FSRQ) and BL Lacs has been discovered. A different shape in the overall energy distributions from radio to γ–ray energies between FSRQ and BL Lacs is also implied by the correlation of their broad–band spectral indices α_{ro} and $\alpha_{x\gamma}$. Both the above correlations can be explained if both the IR to UV emission and the hard X–ray to γ–ray emission originate from the same electron population, via, respectively, the synchrotron process and the inverse Compton mechanism. We suggest that a key parameter for understanding the overall energy distributions of both classes of objects is the energy at which the synchrotron emission peaks in a $\nu - \nu F(\nu)$ representation.

Subject headings: quasars:general – BL Lacertae objects: general – X–rays:galaxies – X–rays:general

1. Introduction

The most important result of the CGRO–EGRET instrument in the field of extragalactic astronomy is the discovery that blazars (i.e. Flat Spectrum Radio Quasars (FSRQ) and BL Lac objects) emit most of their bolometric luminosity in the high γ–ray (E > 100 MeV) energy range.

At present more than 60 blazars detected by EGRET have been identified (Fichtel et al. 1994; von Montigny et al. 1995; Thompson et al. 1995; Nolan et al. 1996; Sreekumar et al. 1996; Lin et al. 1996; Dingus et al. 1996). The majority are FSRQ while about a dozen are classified as BL Lac objects. Furthermore, the Whipple observatory detected 3 BL Lac objects above 300 GeV: Mkn 421 (Punch et al. 1992); Mkn 501 (Quinn et al. 1996) and PKS 2344+514 (Fegan 1996), the latter two not yet detected by EGRET.

The origin of this high energy, strong and variable emission is still not clear. The very nature of the detected sources, all of them being associated with blazars, strongly suggest that relativistic motion and beaming of the emitted radiation are required.

The blazars broad–band energy distribution (BBED) from radio to γ–ray energies, in a ν–νF_ν representation can be characterized by two peaks: one in the IR to UV band and the second in the MeV–GeV band. The smooth rise from radio to infrared frequencies is followed by a cut-off in the optical-UV range with a minimum in the X–ray range. In some objects, in the X–ray band there is an upturn towards higher energies, suggestive of a connection with the peak of the energy distribution in the γ–ray range.

The observed BBED, previously modeled by Comastri, Molendi & Ghisellini (1995, hereinafter Paper I) for a small sample of BL Lac objects and by Sambruna, Maraschi & Urry (1996) for a larger sample of blazars, suggests that the radio to the UV emission is produced by the synchrotron process, while the inverse Compton mechanism is responsible for the high energy γ–ray emission. However, the origin of the seed photons and the location and size of the emitting region(s) are unknown. Seed photons can be produced internally to the emitting blob or jet (by synchrotron emission, as in the jet model of Maraschi, Ghisellini & Celotti, 1992), or be produced externally, by the accretion disk (as in the model of Dermer & Schlickeiser, 1992), by the broad line region illuminated by the disk (as in the model of Sikora, Begelman & Rees, 1994), and/or by some scattering material surrounding the jet (Blandford & Levinson, 1995). Finally, the blob itself could illuminate a portion of the broad line clouds, whose reprocessed line radiation can dominate the radiation energy density in the blob (as in the model of Ghisellini & Madau, 1996).

The main purpose of the present work is to study, for a sizeable sample of bright γ–ray sources, the role of the X–ray emission with respect to the BBED, with particular emphasis on the relation between the X and γ–rays.

The soft X–ray band lies where both synchrotron and self–Compton components are expected to provide a significant contribution to the total emission. For most of the sources, the X–ray flux density allows to estimate the minimum of the BBED, and hence to derive physical parameters to

constrain the theoretical models (synchrotron–self–Compton, hereinafter SSC, Comptonization of ambient radiation field). Further constraints on the emission mechanisms can be obtained from the variability pattern and the slope of the X–ray spectrum. In fact a steep X–ray spectrum is expected if the emission is mainly due to the synchrotron process; in this case the X–ray data coupled with the radio to UV spectrum allow the measurements of the peak of the BBED and the determination of the physical parameters of the synchrotron emission. Rapid flux and spectral variability is expected in this case. Viceversa, a flat X–ray spectrum, expected if the emission is dominated by the Compton flux, suggests that the same process is producing both the X– and γ–ray components, which therefore should show correlated variability patterns.

The outline of the paper is as follows: in Section 2 the sample selection is briefly presented; in Section 3 the analysis of all the available PSPC observations of γ–ray blazars is described in some detail; in Section 4 the correlations among the derived X–ray spectral properties and other bands are illustrated; in Section 5 the origin of the γ–ray emission and its connection with the X–rays is discussed; a summary of the main conclusions is presented in Section 6.

2. The sample

A list of γ–ray blazars has been compiled collecting all the data available in the literature up to September 1996 and contains about 60 sources. The γ–ray bright source list has been cross–correlated with the ROSAT PSPC pointed observations public archive. About half (27) of the sources were either the target of pointed observations or in the field of view (within about 40 arcmin) of a different target. For 19 of the sources, which were not observed in pointing mode, ROSAT All Sky Survey (RASS) data were available in the literature (Brinkmann, Siebert & Boller 1994; Brinkmann et al. 1995). Finally we have included 7 more sources with X–ray fluxes retrieved from missions other than ROSAT.

This selection yielded 53 bright γ–ray blazars which are listed in Table 1. We give the IAU name (col. 1) and other names (col. 2) of the sources, their classification (col. 3), redshift (col. 4), significance of the EGRET detection (col. 5) of the chosen viewing period (col. 6), the reference for the γ–ray data (col. 7), the type of the X–ray observation (col. 8) and its reference (col. 9). A concern regards the selection of the γ–ray data, given the large amount of available observations and analyses of the same data by different authors. For most of the objects there exist several EGRET observations and/or for some of these more than one analysis is available. In these cases we have chosen the γ–ray flux and spectral slope according to the following criteria:

i) spectral index and flux referring to the same observation, ii) data corresponding to a single observing period, iii) when the same data are analyzed by different authors, the results of the most recent analysis are preferred.

Even though not complete, this sample includes about 80 % of all known γ–ray blazars and therefore we feel justified in considering it representative of the entire population.

3. ROSAT Observations and data analysis

3.1. Data reduction

The data reported here are from observations carried out with the ROSAT X–ray telescope (Trümper 1983) with the PSPC in the focal plane (Pfeffermann et al. 1986). The PSPC provides a bandpass in the range $\sim$ 0.1–2.4 keV over a $\sim 2^\circ$ diameter field of view, with a moderate spectral resolution. Most of the observations have been performed in the "wobble" mode. In this mode the detector is moved from the pointing direction with a period of $\sim$ 400 s and an amplitude of $\sim$ 3 arcmin. In this way the effect of shadowing of the X–ray sources by the detector window structures like struts and wire mesh is minimized.

The spatial profiles of the images for all the observations in the $\simeq$ 0.1–2.4 keV range are consistent with those of point sources convolved with the PSPC point spread function (PSF) according to the source spectral properties and keeping into account the background level. Source spectra were extracted from circular regions with radii large enough (from 2 to 4 arcmin) to ensure that all the soft counts be included, given the electronic ghost imaging which widens the PSF below $\sim$ 0.2–0.3 keV (Hasinger et al. 1992). Background spectra were taken either from annulii centered on the sources or from circular regions uncontaminated by nearby sources with extraction radii as large as 10 arcmin. The large extraction cells ensure a good statistics for the modelling of the background spectrum and allow to average the background small scale spatial fluctuations. Different background regions for each source have been extracted and compared. In all the cases the background was stable without any appreciable variability within the statistical errors. Corrections were included for vignetting, especially important for the off–axis sources, and PSPC dead time. The ROSAT observation log is shown in Table 2. The reported count rates are in pulse invariant (PI) channels and are background subtracted. The lowest channel used was 11, as the detector response matrix is not calibrated below this channel, the highest channel depends on the source spectrum and the signal–to–noise ratio of the observation, ranging from channel 200 to 240. A major concern in the analysis of X–ray spectra is the uncertainty in the PSPC response matrix calibration. Actually two matrices have been officially released in order to take into account the $\sim$ 60 Volts gain change applied on October 14, 1991. The first matrix (MPE No. 06) has been adopted for the observations carried out before this date (PV and AO1 targets), while the latest release (MPE No. 36) has been used for all the other observations. The photon event files were analysed using the EXSAS/MIDAS software (version 94NOV, Zimmermann et al. 1993) and the extracted spectra were analysed using version 9.0 of XSPEC (Shafer et al. 1991).

For some of the sources in our sample X–ray data have been previously published by different authors. In order to ensure a uniform procedure for all the sample we have re–analysed all of them obtaining consistent results. For two of the sources in our sample (1226+023≡3C 273 and 1253–055≡3C 279) several tens of pointed observations are available in the public archive as they were the subject of simultaneous multiwavelength campaigns. In this case we have chosen only one (the longest) pointing in order to derive the spectral parameters.

3.2. Spectral Analysis

All the 27 sources have been clearly detected with enough counts to allow spectral analysis. The source spectra were rebinned in order to obtain a significant S/N (> 5) for each bin and fitted with a single power–law model ($F_\nu \propto \nu^{-\alpha}$ where α is the energy spectral index) plus absorption arising from cold material with solar abundances (Morrison & McCammon 1983). The derived spectral parameters are given in Table 3, where the reported errors are at 90 per cent confidence level (Lampton, Margon & Bowyer 1976). All the spectra were fitted with i) the column density fixed at the Galactic value, ii) and free to vary. Accurate values for the Galactic column densities towards most of the objects in our sample have been retrieved from 21 cm radio surveys (Elvis, Lockman & Wilkes 1989; Lockman & Savage 1995; Murphy et al. 1996). The typical error in such measurements is estimated to be of the order of $\simeq 1 - 3 \times 10^{19}$ cm^{-2}. For the remaining objects the Galactic column density values are from Dickey & Lockman (1990). The errors in this case are of the order of $\simeq 1 \times 10^{20}$ cm^{-2}.

It should be noted that radio observations only detect interstellar atomic hydrogen and not molecular gas (i.e. H_2, CO, etc.). Therefore the total effective absorbing column density could be underestimated by 21 cm measurements. Given this possibility we checked for Galactic CO emission in the direction of all the blazars in our sample. Carbon monoxide emission has been detected in the direction of two of the objects in our sample namely: 0528+134 and 2251+158 (Liszt & Wilson 1993; Liszt 1994). Accurate measurements of the CO profile intensity have been recently obtained by Liszt (1996; private communication) as 2.15 K km/s for 0528+134 and 0.77 K km/s for 2251+158.

The molecular hydrogen column density depends on the assumed CO–to–H_2 conversion factor. For 0528+134 a rather conservative assumption of 3×10^{20} molecules cm^{-2} K^{-1} km^{-1} s (Strong et al. 1988) yields an equivalent molecular hydrogen column density N(H_2) $\simeq 1.3 \times 10^{21}$ cm^{-2}, which combined with the atomic value of 2.8×10^{21} cm^{-2} (Dickey & Lockman 1990) gives a total absorbing column of $\sim 4.1 \times 10^{21}$ cm^{-2}.

Given the relatively high Galactic latitude of 2251+158 ($bII \simeq -40°$) a much lower conversion factor of 0.5×10^{20} molecules cm^{-2} K^{-1} km^{-1} s has been assumed (see De Vries, Heithausen & Thaddeus 1987). The molecular hydrogen column density of $\simeq 0.77 \times 10^{20}$ cm^{-2}, combined with the atomic value of 7.06×10^{20} cm^{-2} (Murphy et al. 1996) gives a total absorbing column of 7.83×10^{20} cm^{-2}.

In most cases a single power law spectrum with the absorption fixed at the Galactic value provides an excellent description of the data, while for some of the objects either the fits are statistically unacceptable and/or the column density inferred from the fit is not consistent with the Galactic value, even considering the errors on the Galactic N_H (see column 6 in Table 3), thus requiring a more complex description of the spectral shape.

A double–power–law model has been fitted to all these objects and the results are reported in

Table 4. We point out that for all of the objects the improvement with respect to the single power law fit with $N_H \equiv N_H^{Gal}$ is statistically significant, as indicated by the F–test, at $> 99.9\%$ level.

On the basis of the analysis presented in this subsection it appears that a two component (i.e. a double–power–law) model is required to describe the soft X–ray spectrum for some of the objects, usually the ones with the highest counting statistics in the sample. It is suggested that deeper and/or broader band ($\sim$ 0.1–10 keV) observations will reveal spectral complexity for other objects.

3.3. Statistical Analysis

The range of measured values of the energy spectral indices is large, going from $\simeq$–0.3 to 2.3. We find a significantly different distribution of spectral indices between BL Lacs and FSRQ, as can be clearly seen from the histogram shown in Figure 1. The mean spectral properties have been computed assuming the slopes derived with $N_H \equiv N_H^{Gal}$ if the X–ray absorption is consistent with the Galactic value (col. 3 in Table 3), while the slopes derived from the fit with N_H free have been adopted in the other cases (col. 7 in Table 3). This choice allows a better estimate of the continuum shape for the objects showing either intrinsic absorption or soft excess emission (cfr. Table 4). We have also included the FSRQ 1156+295 using the 2–10 keV *Ginga* slope (Lawson & Turner 1996). When more than one observation was available (see Table 2) a weighted mean spectral slope for each object has been adopted.

A method for estimating the mean and the intrinsic dispersion of the parent population is the maximum–likelihood algorithm (see Maccacaro et al. 1988). The algorithm assumes that the intrinsic distribution of energy indices is Gaussian, and allows the determination of the mean α, the intrinsic dispersion σ, and the respective errors, weighting the individual energy indices according to their measured errors. The results are as follows:

$$\text{BL Lacs :} \qquad \langle \alpha_X \rangle = 1.43 \pm 0.21; \quad \langle \sigma_{\alpha_X} \rangle = 0.43^{+0.22}_{-0.12}$$

$$\text{FSRQ :} \qquad \langle \alpha_X \rangle = 0.67 \pm 0.13; \quad \langle \sigma_{\alpha_X} \rangle = 0.29^{+0.14}_{-0.07}$$

where the confidence intervals are at the 90 per cent confidence level for one interesting parameter.

In order to test if the obtained values are dominated by the brightest sources a simple unweighted mean has been computed. The obtained values: $\langle \alpha_x \rangle = 0.63$, $\sigma = 0.23$ for the 16 FSRQ, and $\langle \alpha_x \rangle = 1.43$, $\sigma = 0.50$ for the 12 BL Lacs objects, where σ is the dispersion on the mean index, are consistent with the maximum likelihood analysis.

The two means are significantly different at $> 99.99\%$ level according to a Student t–test and

taking into account the unequal variances of the two populations. A Kolmogorov–Sminorv (K–S) test for the distribution of the observed values gives almost identical results for the significance of the difference between the two populations (> 99.99 %).

The obtained results indicate that the X–ray spectra of BL Lacs objects are steeper than FSRQ as first suggested by Worral & Wilkes (1990), and that the intrinsic distribution of spectral indices is not consistent with a single value.

Among the BL Lac objects present in our list, 4 are classified as X–ray type BL Lacs (1101+384, 1652+398, 2005–489 and 2155-304), according to their radio to X–ray flux ratio (Padovani & Giommi 1995). The mean X–ray slope for these 4 objects is 1.75±0.33, while for the remaining 8, radio–selected type BL Lacs, we find $\langle \alpha_X \rangle = 1.26 \pm 0.46$. Despite the low number of X–ray type BL Lacs, the two slopes are different at > 96.6 % as indicated by the Student t–test, in agreement with our previous results (Paper I).

3.4. Temporal analysis

The background–subtracted light curves have been computed for each source. As suggested by the wobble period of the telescope the collected photons were binned in 400 or 800 s time intervals depending on the source counting statistic. The binned light curves for each source were fitted with a constant value. The probabilities associated to the χ^2 statistic suggest that, in most of the cases, the light curves are not variable over the full observation with maximum deviations of the order of 20–30 %. Given that a detailed study of relatively small amplitude (< 50 %) variability is extremely difficult for sources observed on–axis due to the source obscuration from the fine wires mesh of the PSPC window (Hasinger, private communication), variations of this order could be entirely due to instrumental effects.

Large flux variability on short timescales (< 1 day) has been detected only in S5 0716+714 which is discussed in a separate paper (Cappi et al. 1994). Variations within the same PSPC observation are present in two more objects: 0219+428 ≡ 3C 66 A and PKS 2155–304.

For 0219+428 the count rate decreased by about a factor 2 on a timescale of ~ 3.5 days without any significant spectral variability. In the bright BL Lac object PKS 2155–304 an increase of a factor ~ 1.7–1.8 on a timescale of ~ 2.4 days has been detected. Given the high number of accumulated counts a time resolved spectral analysis was possible. From an inspection of the light curve two states can be clearly identified: a low state at the beginning of the observation with a mean count rate of ~ 28 counts s^{-1} and a high state (~ 48 counts s^{-1}) at the end of the observation. In both cases a single power law with absorption fixed at the Galactic value provide a good description of the observed spectrum, which flattens from $\alpha = 1.42 \pm 0.05$ in the low state to $\alpha = 1.28 \pm 0.02$ in the high state, with a behaviour typical of BL Lac objects.

Finally, large amplitude (up to a factor 3) flux variability has been observed for some of the

sources in the sample for which several observations were available in the public archive (Table 2). The observed timescales range from a few days to several months. For two objects (0851+202 $\equiv$ OJ 287 and 2005–489) spectral variability has been detected as well. For a detailed discussion of the spectral variability in PKS 2005−489 we refer to Sambruna et al. (1995). For OJ 287 a spectral steepening ($\Delta\alpha \simeq 0.4 - 0.5$) between the first two observations separated by about 7 months, is associated with a doubling count rate. A further observation, after two years, reveals a count rate comparable to the second observation, but a slope similar to the first.

4. γ–ray and overall spectral properties

4.1. γ–ray energy distribution

In Table 5 we list the γ–ray fluxes for all the sources in our sample, together with spectral indices if available. With the same maximum–likelihood algorithm applied in Section 3.3 we have computed the mean γ–ray slope for BL Lacs (10 out of 16 objects) and FSRQ (30 out of 37 objects); the results are as follows:

$$\text{BL Lacs}: \qquad \langle\alpha_\gamma\rangle = 0.87 \pm 0.13; \quad \langle\sigma_{\alpha_\gamma}\rangle < 0.26$$

$$\text{FSRQ}: \quad \langle\alpha_\gamma\rangle = 1.25 \pm 0.10; \quad \langle\sigma_{\alpha_\gamma}\rangle = 0.25^{+0.10}_{-0.07}$$

where the confidence intervals are at 90 per cent level for one interesting parameter. The fact that the intrinsic dispersion of BL Lac spectral indices is consistent with zero is probably due to the small number of objects.

A simple unweighted mean returns almost identical values: $\langle\alpha_\gamma\rangle = 1.29$, $\sigma = 0.34$ for FSRQ, and $\langle\alpha_\gamma\rangle = 0.87$, $\sigma = 0.32$ for BL Lacs where σ is the dispersion on the mean index.

The two means are significantly different at $> 99.7\%$ level according to a Student t–test. Similar results (> 99.8 %) for the significance of the difference between the two populations are returned from a K–S test on the distribution of the observed values.

The distributions of spectral indices indicate an opposite behaviour at γ–ray energies with respect to the X–ray band (Figure 1). For the subsample of 23 objects for which both X– and γ–ray spectral slopes are available, a significant, at $> 98.6\%$ level using a non–parametric Spearman rank test, anti–correlation has been found between the two spectral indices (Figure 2) when both FSRQ and BL Lacs are considered. The correlation is however much weaker considering FSRQ only (82 %) and is not present for BL Lacs only (15 %). FSRQ and BL Lacs occupy two different regions in the α_x–α_γ plane. A flat X–ray spectrum is thus associated with a steep γ–ray slope for FSRQ while the reverse is true for BL Lacs. A similar correlation was found by Wang, Luo & Xie

(1996) with a smaller sample (10 objects) and inhomogeneus X–ray data.

These findings suggest that either the α_x–α_γ correlation is just the result of a fortituous proximity of the locii occupied by BL Lacs and FSRQ in the α_x–α_γ plane, or the correlation points to an underlying physical mechanism operating in both classes of objects.

4.2. Broad–band energy distribution

Radio and optical data for all the 53 objects in our sample have been collected from the literature in order to characterize the BBED (Table 5). Since the γ–ray detection is likely to be associated with a high state of the source we have chosen to list the brightest radio and optical fluxes, the latter corrected for reddening.

We have computed the broad band spectral indices α_{12} defined as $-log(L_2/L_1)/log(\nu_2/\nu_1)$ where L_1 and L_2 are the rest–frame luminosities observed at the frequencies ν_1 and ν_2, where ν_R = 5 GHz, ν_O = 5500 Å, ν_x = 1 keV and ν_γ = 100 MeV. The K–correction has been applied using the listed values of α_x and α_γ whenever available and the mean spectral indices for BL Lacs and FSRQ derived in the previous sections (cfr. § 3.2.1 and § 4.1) for sources with unknown spectra. Finally, $\alpha_R = 0$ and $\alpha_O = 1$ have been assumed at radio and optical frequencies.

A highly significant anti–correlation, (at > 99.99 % using a non–parametric Spearman rank test), has been found between α_{ro} and $\alpha_{x\gamma}$ (Figure 3), when considering the entire class of blazars. A similar level of significativity is present applying a bi–dimensional K–S test (see Press et al. 1992). The correlation persists for each class of objects, although with less significance (99.3% for BL Lacs and 96.9% for FSRQ).

Moreover, BL Lacs and FSRQs occupy different regions of the α_{ro}–$\alpha_{x\gamma}$ plane. A relatively steep radio to optical spectral index implies a flat X to γ–ray flux ratio and is common among FSRQ, while the opposite is true for BL Lac objects. The average values are as follow:

$$\text{BL Lacs}: \qquad \langle\alpha_{ro}\rangle = 0.47 \pm 0.12; \quad \langle\alpha_{x\gamma}\rangle = 0.83 \pm 0.18$$

$$\text{FSRQ}: \quad \langle\alpha_{ro}\rangle = 0.69 \pm 0.10; \quad \langle\alpha_{x\gamma}\rangle = 0.58 \pm 0.12$$

Even if the broad band indices α_{ro} and $\alpha_{x\gamma}$ are independent quantities, so that the effects of spurious correlations are minimized, the observed correlation could be induced by other variables such as redshift and/or luminosity.

Indeed significant correlations (at > 99.9 %) have been found between both $\alpha_{x\gamma}$ and α_{ro} with redshift and γ–ray luminosity. This is not surprising given that BL Lac objects have, on average, lower luminosities and redshifts, compared to FSRQ.

The dependence on redshift and luminosity in the α_{ro}–$\alpha_{x\gamma}$ correlation can be removed applying a partial correlation analysis (Kendall & Stuart 1979). The results indicate that excluding the effect of z, the α_{ro}–$\alpha_{x\gamma}$ correlation is significant at the 99.1 % level. By the same partial correlation analysis, we have investigated the dependence of the α_{ro}–$\alpha_{x\gamma}$ correlation upon the γ–ray luminosity L_γ. The significance, excluding the effect of L_γ, decreases to the 97.2 % level. Therefore we conclude that the α_{ro}–$\alpha_{x\gamma}$ correlation is not induced by redshift and it is significant even when considering the dependence on L_γ, which however plays a relatively important role.

These findings coupled with the α_x–α_γ relation described in § 4.1 points to an underlying physical mechanism linking the two classes of objects.

5. Discussion

5.1. One or two electron population?

The overall $\nu F(\nu)$ spectrum of blazars shows two peaks: the low energy one at IR/soft X–ray energies, and the high energy one peaking in the MeV/GeV range. These two peaks can be due to a *single* population of electrons, emitting synchrotron and inverse Compton radiation, or can be the result of the emission of *two* different electron populations, emitting both by the synchrotron process, as in the 'proton blazar' model of Mannheim (1993). In the former case (one population), the two frequencies at which the overall emission peaks are obviously related, being produced by the same electrons. This holds whatever is the origin of the seed photons to be upscattered at higher energies. If this is the case, then one expects correlations between fluxes and slopes in different energy bands, of the kind found in the present paper, between the slopes at X–rays and γ–ray energies, and between the broad band spectral indices connecting the radio with the optical, and the X–ray with the γ–rays.

To illustrate our findings, we plot in Fig. 4 the overall spectra of two blazars: the low redshift BL Lacertae object Mkn 421, and the high redshift low polarized quasar 0836+710. As can be seen, both peaks (synchrotron and inverse Compton peaks) are at smaller energies for 0836+710, and in this object the γ–ray luminosity is more dominant. We have chosen these two sources because they are representative of the two classes and have very different BBEDs.

Note that the X–ray emission of Mkn 421 connects smoothly with the lower energy part of the spectrum, suggesting that in this source the X–rays are due to the synchrotron mechanism. This implies the presence of very energetic electrons, whose inverse Compton emission can then account for the observed emission in the TeV band. Instead, the BBED of 0836+710 suggests that the synchrotron peak occurs in the IR part of the spectrum, indicating that the electrons radiating at this peak have smaller energies than in the Mkn 421 case. As a result, the high energy peak should move to the MeV range. The extrapolations of the steep γ–ray and the flat X–ray spectra indeed form a peak at a few MeV.

The found anti–correlation between α_X and α_γ can be easily interpreted in the 'one electron population' scenario. Steep X–ray spectra smoothly connecting with lower frequencies emission imply synchrotron radiation and therefore a high frequency for the 'Compton' peak, possibly beyond the EGRET band is expected. This in turn implies flat γ–ray slopes.

This scenario can also account for the anti–correlation between α_{ro} and $\alpha_{x\gamma}$. As in Mkn 421 (Figure 4) a flat α_{ro} occurs when the synchrotron component peaks at frequencies above the optical band. This implies a large X–ray flux, due to synchrotron emission, and a relatively small 100 MeV flux, since the peak of the γ–ray emission is above 100 MeV: as a consequence, flat α_{ro} imply steep $\alpha_{x\gamma}$ indices.

The idea of an energy break moving from X–ray to optical–infrared frequencies and related to the maximum energy of relativistic electrons has been suggested by Padovani & Giommi (1995) in order to explain the difference between radio and X–ray selected BL Lac objects. Indeed this idea, modified to take into account the relation between the frequency of the 'synchrotron peak' (ν_S) and the bolometric synchrotron luminosity, can explain the different numbers of X–ray and/or radio bright BL Lac objects selected from flux limited surveys, their different redshift distributions and evolution (Fossati et al. 1996). A continuity of properties among the various classes of blazars has been also suggested by Sambruna et al. (1996) from a multiwavelength analysis of sources (mainly BL Lac objects) detected with the ROSAT PSPC. The inclusion of the γ–ray data available by definition in our sample, allowing to study the BBED over a much broader energy range, confirms and extends these findings (see also Padovani & Giommi 1995; Sambruna et al. 1996; Maraschi et al 1995).

In the case of *two* electron populations an explanation of all these findings would require a fine tuning between the extension in energies and total energy content of the two distributions.

Futhermore, the coordinated variability of the optical and γ-ray flux (Maraschi et al. 1994 and Hartman et al. 1996 for 3C 279; Wagner et al. 1995 for 1406–076) can be naturally accounted for by a *"single"* population model, while in the case of *two* electron distribution scenario the correlated variability would require a even tighter tuning.

We then conclude that one electron population is a simpler explanation of the BBED of γ–ray bright blazar, with respect to the proton blazar scenario. If true, this means that the overall synchrotron behaviour at IR–UV frequencies (peak energy and variability) allows to predict the behaviour at high energies: by monitoring blazars in the optical UV we therefore monitor the same electrons making the high energy emission.

Note that the α_{ro}–$\alpha_{x\gamma}$ relation suggests that the more γ–ray dominated sources are on average optically faint and are also expected to have a steep spectrum in the infrared–optical range. If this is the case, relatively bright γ–ray sources could then be discovered among red FSRQ. We point out that the source with the steepest α_{ro} (and the flattest α_x) in our sample (i.e. 0202+149) shows an extremely red optical–infrared spectrum without any evidence of reddening (Stickel et al. 1996). A selection based on optical colors may provide a starting sample for future more sensitive

γ–ray missions (i.e. GLAST).

5.2. Implications on the emission models

A single population of electrons can produce the entire BBED of blazars by the synchrotron and the inverse Compton process. However, as mentioned in the introduction, we still do not know the origin of the seed photons for the inverse Compton process.

As noted in Dondi and Ghisellini (1995), the γ–ray emission in BL Lacertae objects is less dominant than in FSRQ, even if it extends to higher energies. Together with the absence of emission lines, this suggests that the main radiation mechanism in BL Lacertae objects is the synchrotron self–Compton (SSC) process. The (very approximate) equality of the luminosity of the two components suggests that the magnetic field is close to equipartition with the synchrotron radiation energy density. We then applied a one–zone homogeneous SSC model to the overall emission of Mkn 421, for which simultaneous data are available both for a 'quiescent' state and a flaring state (Macomb et al. 1995) with the parameters listed in Table 6. A similar model has been applied in Ghisellini, Maraschi & Dondi (1996). We have assumed that in a spherical source of size R electrons are continuously injected, between γ_{min} and γ_{max}, with a power law distribution function, corresponding to an injected (intrinsic) luminosity L_{inj} and a compactess $\ell_{inj} \equiv \sigma_T L_{inj}/(Rmc^3)$. The steady particle distribution, responsible for the emission, is found self-consistently, through a continuity equation, by balancing the injection rate with the cooling rate, and taking into account Klein Nishina effects, pair production and adiabatic losses (Ghisellini, 1989). As can be seen, both states of the source can be reproduced by varying only the injected luminosity (by a factor 2), and γ_{max} (by almost a factor 3). Incomplete synchrotron and inverse Compton cooling is responsible for the curved spectral energy distribution, even if the injected electron distribution function is a single power law in the entire energy range. As a result, the electrons responsible for most of the emitted radiation (both in the synchrotron and the inverse Compton peaks) have Lorentz factor close to $\gamma_p = 3 \times 10^5$ in the high state, and 3 times less in the low state.

For 0836+710, we have applied both the SSC model and the 'external Compton' model (EC), as developed by Sikora et al. (1994). The input parameters are listed in Table 6. In this EC scenario, we have assumed that the radiation produced external to the jet is dominating the electron cooling, and is distributed in energy as a diluted blackbody, peaking in the UV band.

Note that both models account for the main characteristics of the overall emission of 0836+710. On the basis of the pure BBED, therefore, one cannot discriminate among the two models. Other information, such as the broad line luminosity, and the variability pattern in the IR–UV band with respect to the γ–ray band, is necessary in order to select which are the dominant seed photons for the inverse Compton process.

In both models for 0836+710, the injected electron distribution function must have a

low energy cut–off, resulting in a double power law steady particle distribution. The curved synchrotron and inverse Compton spectra are due to the form of the injection function, and not to the incomplete cooling of the electrons. In this case most of the emission at both the synchrotron and Compton peaks is produced by electrons with Lorentz factors close to γ_{min}. The equilibrium steady particle distribution is in fact a double power law, with a break at $\gamma_p = \gamma_{min}$. Its value, both for the SSC and the EC case, is lower than the corresponding γ_p in Mkn 421.

The main difference between the SSC and the EC models for 0836+710 concerns the value of the magnetic field, which is close to equipartition with the synchrotron radiation energy density in the EC case, and much weaker in the SSC case.

Despite the fact that both models can fit the data of 0836+710, we can nevertheless draw the conclusion that the different BBEDs of Mkn 421 and 0836+710 are mainly due to a difference in the value of their typical electron energies γ_p. A distribution of γ_p, therefore, could well be responsible for the observed variety of BBEDs of blazars.

5.3. BL Lacertae objects versus FSRQ

As extensively discussed in the previous sections BL Lacertae objects differ from FSRQ as: i) they tend to have steeper X–ray and flatter γ–ray spectra; ii) they separate from FSRQ in the α_{ro}–$\alpha_{x\gamma}$ plane. Moreover Dondi & Ghisellini (1995) found that: iii) the ratio between the γ–ray and optical luminosity, $L\gamma/L_o$, which can be considered as a measure of the 'γ–ray dominance', is of the order of unity in BL Lacertae objects, and much greater in FSRQ. We confirm this result with our larger sample, deriving $< L_\gamma/L_o > \simeq 1$ for BL Lacertae objects and $< L_\gamma/L_o > \simeq 30$ for FSRQ.

We have already argued that points i) and ii) can be explained if the overall spectrum is produced by a single population of electrons whose distribution is characterized by a break energy γ_p, which is, on average, smaller in FSRQ with respect to BL Lacertae objects. Point iii) above suggests that the value of γ_p may be related to the ratio of the Compton to synchrotron luminosity: the smaller γ_p, the larger the Compton dominance. This can also explain the found dependence of the α_{ro}–$\alpha_{x\gamma}$ correlation upon L_γ.

We speculate that this may be related to the electron Compton cooling rate. In less compact sources, with no important emission lines, the electron cooling time is long. Large values of γ_p are then possible as a result of a competition between acceleration and cooling rates, or, alternatively, between cooling and adiabatic expansion (or particle escape) rates.

The fact that BL Lacertae objects have no or weak emission lines then suggests that one key parameter to explain the BBED of all objects is the relative importance of the broad emission lines. If present, they can contribute significantly to the Compton cooling, resulting in small value of γ_p and a dominating γ–ray emission. If absent, the γ–ray emission is instead ruled by the

synchrotron radiation energy density, with a relatively lower γ–ray dominance and larger γ_p.

We stress that this is only one of the possible ideas trying to explain the overall energy distribution in blazars, but has the advantage, besides its semplicity, to unify the spectral properties of all blazars on the basis of one parameter: the dominant Compton cooling agent. We will investigate this idea in a future paper.

6. Conclusions

We have analysed ROSAT PSPC data for 27 bright EGRET and Whipple sources, X–ray fluxes for further 26 sources have been retrieved from the ROSAT All Sky Survey and from other X–ray missions. The main conclusions can be summarized as follow:

(1) The measured X–ray spectra show a very broad distribution with energy indices in the range $\alpha \sim -0.3 - 2.3$. In the soft $\sim$ 0.1–2.0 keV X–ray band the mean spectral slope of BL Lac objects is significantly steeper than the mean slope of FSRQ. The reverse is true in the γ–ray band where FSRQ spectra are steeper than BL Lac ones.

(2) Significant anti–correlations have been found between α_x and α_γ and α_{ro} and $\alpha_{x\gamma}$. The distribution of BL Lacs and FSRQ in these two diagrams (Figures 2 and 3) suggests that the two classes of objects represent the extremes of a continuous distribution rather than two distinct populations. These correlations can be explained if the same relativistic electrons are responsible for both the radio to optical and the hard X to γ–ray emission, via, respectively, the synchrotron and the inverse Compton processes.

(3) We suggest that the important parameter in describing the observed BBEDs is the synchrotron peak energy [in a $\nu - \nu F(\nu)$ plot], greater in BL Lac objects than in FSRQ.

(4) We speculate that the proposed distribution in the values of the peak energy of the synchrotron component may be due to the different amount of radiative cooling suffered by the relativistic electrons. More severe radiative cooling would result in a small value of the synchrotron peak energy and a more dominating γ–ray emission.

(5) It is predicted that relatively bright γ–ray sources have red optical colors (or viceversa). Future missions in the γ–ray (i.e. GLAST) and near infrared optical spectrophotometry should be able to test this hypothesis.

We are grateful to H. Liszt who kindly provided recent results on CO absorption values, to O. Bendinelli for useful discussions on statistical analysis tests, to G. Zamorani, G.G.C. Palumbo and M. Cappi for a careful reading of the manuscript. An anonymous referee is thanked for several suggestions resulting in a substantial improvement of the original version of the paper. This work has been partially supported by the Italian Space Agency (ASI–94–RS–96). GF acknowledges

the Italian MURST for financial support. This research has made use of the NASA/IPAC Extragalactic Database (NED) which is operating by the Jet Propulsion Laboratory, California Institute of Technology under contract with the National Areonautic and Space Administration.

REFERENCES

Becker, R.L., White, R.L. & Edwards, A.L. 1991, ApJS, 75, 1

Bertsch, D.L., et al. 1993, ApJ, 405, L21

Blandford, R.D., & Levinson, A. 1995, ApJ, 441, 79

Boznyan, E.P., Hemenway, P.D., & Argue, A.N. 1990, AJ, 99, 1421

Brinkmann, W., Siebert, J., & Boller, T. 1994, A&A, 281, 355

Brinkmann, W., et al. 1995, A&AS, 109, 147

Brunner, H., Lamer, G., Worral, D.M., & Staubert, R. 1994, A&A, 287, 436

Cappi, M., Comastri, A., Molendi, S., Palumbo, G.G.C., Della Ceca, R., & Maccacaro, T. 1994, MNRAS, 271, 438

Comastri, A., Molendi, S., & Ghisellini, G. 1995, MNRAS, 277, 297 (Paper I)

Comastri, A., Cappi, M., & Matsuoka, M., 1996, in Proc. of "Röntgenstrahlung from the Universe", H.U. Zimmermann, J. Trümper, H. Yorke eds., MPE Report 263, 439

Dermer, C., & Schlickeiser, R. 1993, ApJ, 416, 458

de Vries, H.W., Heithausen, A., & Thaddeus, P. 1987, ApJ, 319, 723

Dickey, J.M., & Lockman, F.J. 1990, ARA&A, 28, 215

Dingus, B.L., et al. 1996, ApJ, 467, 589

Dondi, L., & Ghisellini, G. 1995, MNRAS, 273, 583

Elvis, M., Lockman, F.J., & Wilkes, B.J. 1989, AJ, 97, 777

Fegan, D.J. 1996, private communication

Fichtel, C.E., et al. 1994, ApJS, 94, 551

Fossati, G., Celotti, A., Ghisellini, G., & Maraschi, L. 1996, MNRAS, submitted

Gear, W.K. et al. 1994, MNRAS, 267, 167

Ghisellini, G., Maraschi, L., Tanzi, E., & Treves, A. 1986, ApJ, 310, 317

Ghisellini, G. 1989, MNRAS, 238, 449

Ghisellini, G., Maraschi, L., & Dondi, L. 1996, A&AS, 120, in press

Ghisellini, G., & Madau, P. 1996, MNRAS, 280, 67

Giommi, P., Ansari, S.G., & Micol, A. 1994, A&AS, 109, 267

Gregory, P.C., & Condon, J.J. 1991, ApJS, 75, 1011

Griffith, M.R., Wright, A.E., Burke, B.F., & Ekers, R.D. 1994, ApJS, 91, 111

Hartman, R.C., et al. 1993, ApJ, 407, L41

Hartman, R.C., et al. 1996, ApJ, 461, 698

Hasinger, G., Turner, T.J., George, I.M., & Boese, G. 1992, Legacy No. 2

Hewitt, A., & Burbidge, G. 1993, ApJS, 87, 451

Impey, C.D., & Tapia, S. 1988, ApJ, 333, 666

Impey, C.D., & Tapia, S. 1990, ApJ, 354, 124

Kendall, M., & Stuart, A. 1979, The Advanced Theory of Statistic, MacMillian, New York

Kühr, H., Witzel, A., Pauliny–Toth, I.I.K., & Nauber, U. 1981, A&AS, 45, 367

Lampton, M., Margon, B., & Bowyer, S., 1976, ApJ, 208, 177

Lawson, A.J., & Turner, M.J.L. 1996, MNRAS, submitted

Ledden, J.F., & O'Dell, S.L. 1985, ApJ, 298, 630

Lin, Y.C., et al. 1995, ApJ, 442, 96

Lin, Y.C., et al. 1996, ApJS, 105, 331

Liszt, H.S., & Wilson, R.W. 1993, ApJ, 403, 663

Liszt, H.S. 1994, ApJ, 429, 638

Lockman, F.J., & Savage, B.D. 1995, ApJS, 97, 1

Maccacaro, T., Gioia, I.M., Wolter, A., Zamorani, G., & Stocke, J.T. 1988, ApJ, 326, 680

Macomb, D.J., et al. 1995, ApJ, 449, L99

Madejski, G., Takahashi, T., Tashiro, M., Kubo H., Hartman R., Kallman, T., & Sikora, M. 1996, ApJ, 459, 156

Mannheim, K., 1993, A&A, 269, 67

Maoz, D., et al. 1993, ApJ, 409, 28

Maraschi, L., Ghisellini, G., Tanzi, E., & Treves, A. 1986, ApJ, 310, 325

Maraschi, L., Ghisellini, G. & Celotti, A. 1992, ApJ, 397, L5

Maraschi, L., et al. 1994, ApJ, 435, L91

Maraschi, L., Fossati, G., Tagliaferri G., & Treves A. 1995, ApJ, 443, 578

Mattox, J.R., et al. 1997, ApJ, 476, Feb 20 issue (astro-ph/9610007)

Morrison, R., & McCammon, D.,1983, ApJ, 270, 119

Mukherjee, R., et al. 1995, ApJ, 445, 189

Murphy, E.M., Lockman, F.J., Laor, A., & Elvis, M. 1996, ApJS, 105, 369

Nolan, P.L., et al. 1996, ApJ, 459, 100

Padovani, P., & Giommi, P. 1995, ApJ, 444, 567

Pearson, T.J., & Readhead, A.C.S. 1988, ApJ, 328, 114

Perley, R.A. 1982, AJ, 87, 859

Perlman, E.S., Stocke, J.T., Schachter, J., Elvis, M., Ellingson, E., Urry, C.M., Potter, M., Impey, C.D., & Kolchinsky, P. 1996, ApJS, 104, 251

Pfeffermann, E. et al., 1986, in Proc. SPIE 733, Soft X-ray optics and Technology, p. 519

Pian, E., Falomo, R., Scarpa, R., & Treves, A. 1994, ApJ, 432, 547

Pian, E., Falomo, R., Ghisellini, G., Maraschi, L., Sambruna, R.M., Scarpa, R., & Treves, A. 1996, ApJ, 459, 169

Press, W.H., Teukolsky, S.A., Vetterling, W.T. & Flannery, B.P. 1992, Numerical Recipes Second Edition, Cambridge University Press

Preston, R.A., Morabito, D.D., Williams, J.G., Faulkner, J., Jauncey, D.L., & Nicholson, G.D. 1985, AJ, 90, 1599

Punch, M., et al. 1992, Nature, 358, 477

Quinn, J., et al. 1996, ApJ, 456, L83

Rusk, J, & Seaquist, E.R. 1985, AJ, 90, 30

Sambruna, R.M., Urry, C.M., Ghisellini, G., & Maraschi, L. 1995, ApJ, 449, 567

Sambruna, R.M., Maraschi, L., & Urry, C.M. 1996, ApJ, 463, 444

Shafer, R.A., Haberl, F., Arnaud, K.A., & Tennant, A.F. 1991, XSPEC User's Guide, ESA TM–09, Noordwijk, The Netherlands

Shrader, C.R., et al. 1994, AJ, 107, 904

Shrader, C.R., et al. 1996, A&AS, 120, in press

Sikora, M., Begelman, M.C., & Rees, M.J. 1994, ApJ, 421, 153

Sreekumar, P., et al. 1996, ApJ, 464, 628

Stickel, M., Padovani, P., Urry, C.M., Fried, W., & Kühr, H. 1991, ApJ, 374, 431

Stickel, M., Rieke, G.H., Kühr, H., & Rieke, M.J. 1996, ApJ, 468, 556

Strong, A.W., Bloemen, J.B.G.M., Dame, T.M., Grenier, I.A., & Hermsen, W. 1988, A&A, 207, 1

Thompson, D.J., et al. 1993, ApJ, 415, L13

Thompson, D.J., et al. 1995, ApJS, 101, 259

Treves, A., Belloni, T., Falomo, R., Fink, H., Maraschi, L., Sambruna, R.M., Tagliaferri, G., & Zimmermann, H.U. 1993, ApJ, 406, 447

Trümper, J., 1983, Adv. Space Res., 2, 241

Veron–Cetty, M.P., & Veron, P. 1993, ESO Scientific Report no 13

Vestrand, W.T., Stacy, J.G., & Sreekumar, P. 1995, ApJ, 454, L93

von Montigny, C., et al. 1995, ApJ, 440, 525

Wagner, S.J., et al. 1995, ApJ, 454, L97

Wall, J.V., & Peacock, J.A. 1985, MNRAS, 216, 173

Wang, J., Luo, Q., & Xie, G. 1996, ApJ, 457, L65

Wilkes, B.J., Tananbaum, H., Worral, D.M., Avni, Y., Oey, M.S., & Flanagan, J. 1994, ApJS, 92, 53

White, R.L., & Becker, R.H. 1992, ApJS, 79, 331

Worral, D.M., & Wilkes, B.J. 1990, ApJ, 360, 396

Zhang, Y.F., Marscher, A.P., Aller, H.D., Aller, M.F., Teräsranta, H., & Valtaoja, E. 1994, ApJ, 432, 91

Zimmermann, H.U., Belloni, T., Izzo, C., Kahabka, P., & Schwentker, O. 1993, EXSAS User's Guide, MPE Report 244

Fig. 1.— Histograms of the X–ray and γ–ray spectral indices for BL Lacs and FSRQ. The adopted values for the X–ray spectral indices are those listed in Table 5.

Fig. 2.— γ–ray vs X–ray spectral index for the sources in our sample. The adopted values for the X–ray spectral indices are those listed in Table 5. Filled symbols refer to BL Lac objects, empty symbols refer to FSRQ.

Fig. 3.— Correlation between the broad band spectral indices α_{ro} and $\alpha_{x\gamma}$ for the objects in our sample. Filled symbols refer to BL Lac objects, empty symbols refer to FSRQ. X–ray bright BL Lacs (XBL) have been highlighted with their name, they cluster in the lower-right part of the diagram. We have also labelled the object with the steepest α_{RO}. For 1652+398 and 2344+514, which have not been detected by EGRET, we have assumed a γ–ray flux of 0.8×10^{-7} photons cm^{-2} s^{-1}, approximately equal to the sensitivity threshold of EGRET.

Fig. 4.— Two examples of BBEDs illustrating the difference among BL Lac objects and FSRQ. The data have been collected from the literature and the references are reported in Table 5. The overall spectrum of 0836+710 is fitted with the SSC model (solid line) and the EC (external Compton) model (dashed line), as explained in the text. In both cases a simple one–zone homogeneous sphere has been assumed. Input parameters for both models are listed in Table 6. In the EC model, relativistic electrons produce, by synchrotron, the mm to UV emission, while the high energy spectrum is due to inverse Compton scattering off seed photons produced externally to the jet. The "synchrotron" and "Compton" peaks are due to electrons with Lorentz factors $\gamma_p \sim 150$. In the SSC model the 'synchrotron' and the 'Compton' peaks are instead due to electrons with Lorentz factor $\gamma_p \sim 4 \times 10^3$. The soft X–ray data are from the present work, while the 0.5–10 keV spectral parameters have been retrieved from a recent ASCA analysis (Comastri et al. 1996). For Mkn 421, the overall spectra refer to the May 1994 flare (circles) and to the preceding quiescent period (squares) (Macomb et al. 1995). The filled square corresponds to the ROSAT observation analyzed in this paper. The solid and dot-dashed lines refer to one–zone, homogeneous synchrotron self–Compton models (see also Ghisellini, Maraschi & Dondi, 1996), with no contributions from external photons. Input parameters are listed in Table 6. The synchrotron and self Compton peaks are due to electrons of Lorentz factor $\gamma_p \sim 10^5$. The two different spectra are obtained by varying the number of emitting electrons (by a factor 3) and their maximum energy (by a factor 2).

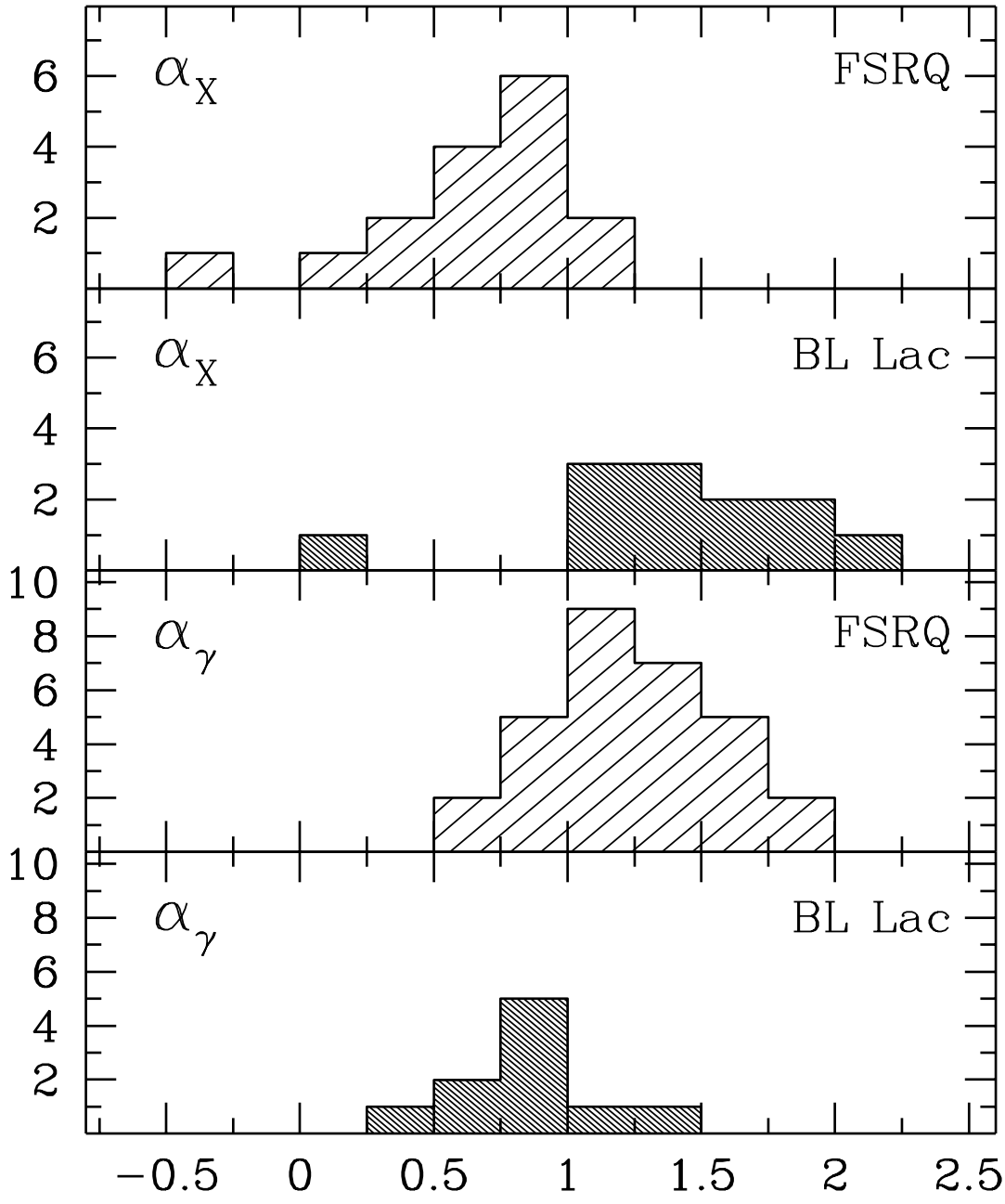
α_X
FSRQ
α_X
BL Lac
α_γ
FSRQ
α_γ
BL Lac
−0.5
0
0.5
1
1.5
2
2.5

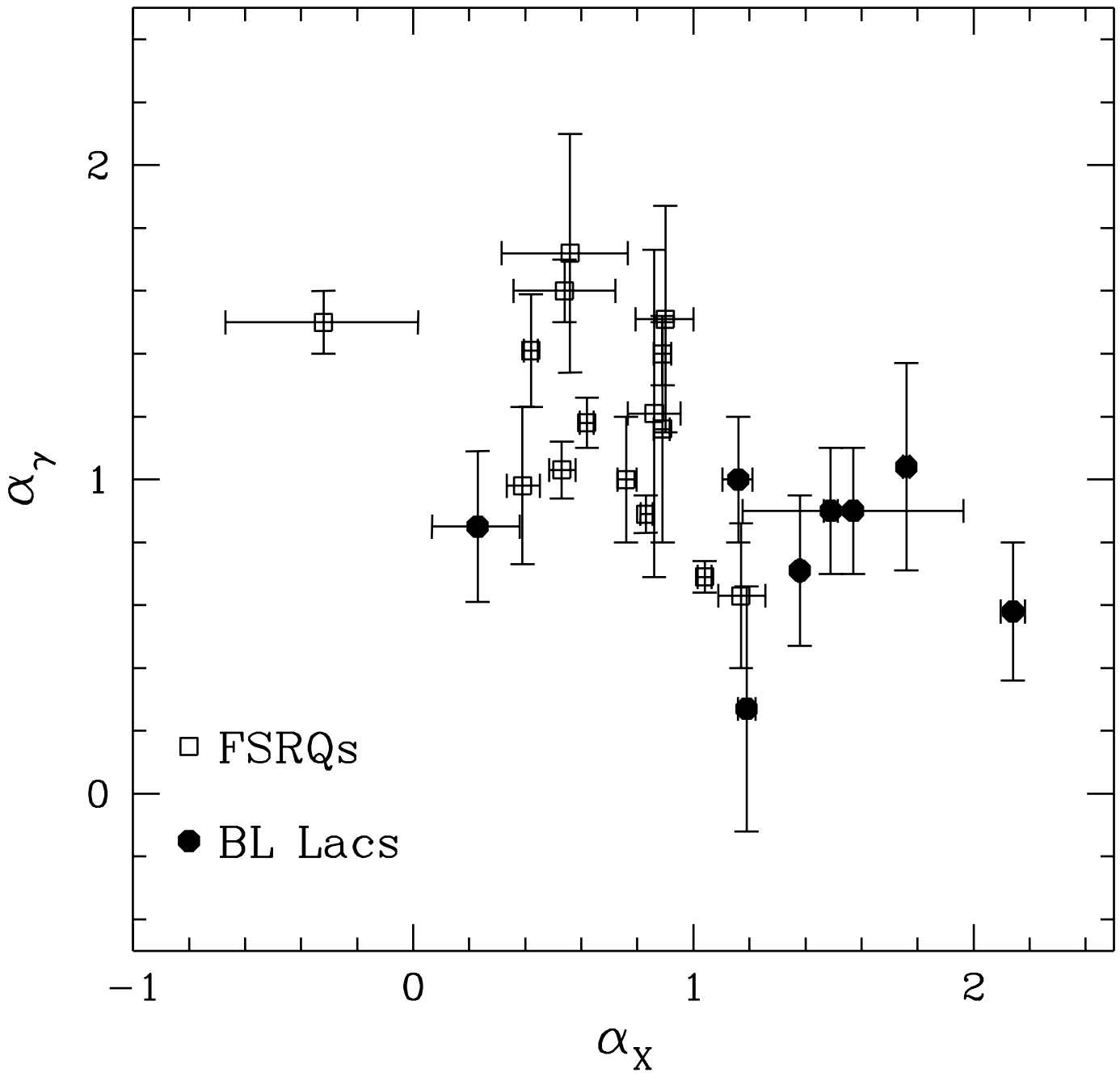
2
1
0
−1
0
1
2
α_γ
α_X
FSRQs
BL Lacs

TABLE 2
ROSAT PSPC Observations of EGRET Sources

Name[a]	ROR[b]	Start Time	Off–axis (arcmin)	exposure (seconds)	count rate (cts/sec)
0202+149	300003p	30/07/91	29.8	25174	0.019 ± 0.002
0208−512[1]	701161p	30/05/93	0.2	1811	0.268 ± 0.013
0208−512[2]	701164p	01/06/93	0.2	1780	0.254 ± 0.012
0208−512[3]	701156p	09/06/93	0.2	2160	0.270 ± 0.012
0208−512[4]	701158p	07/06/93	0.2	2149	0.277 ± 0.012
0208−512[5]	701157p	08/06/93	0.2	2220	0.267 ± 0.012
0208−512[6]	701168p	06/06/93	0.2	2534	0.275 ± 0.011
0208−512[7]	701159p	28/05/93	0.2	2698	0.241 ± 0.010
0208−512[8]	701167p	05/06/93	0.2	2701	0.265 ± 0.010
0208−512[9]	701163p	01/06/93	0.2	2735	0.254 ± 0.010
0208−512[10]	701160p	29/05/93	0.2	4026	0.262 ± 0.009
0208−512[11]	701162p	31/05/93	0.2	1472	0.252 ± 0.014
0208−512[12]	701166p	04/06/93	0.2	1154	0.243 ± 0.015
0219+428[1]	500266p	05/08/93	41.1	31528	0.316 ± 0.005
0235+164[c,1]	701379p	21/07/93	0.2	2083	
	701380p	24/07/93	0.2	1903	
	701381p	26/07/93	0.2	1508	0.293 ± 0.007
0235+164[c,2]	701384p	04/08/93	0.2	2023	
	701385p	06/08/93	0.2	4099	
	701387p	12/08/93	0.2	1664	
	701388p	15/08/93	0.2	1708	0.108 ± 0.003
0521−365	701179p	29/08/92	0.1	4845	0.780 ± 0.013
0528+134[1]	700059p	15/03/91	0.5	3791	0.069 ± 0.005
0528+134[2]	900340p	21/09/92	0.5	4514	0.091 ± 0.005
0537−441	700199p	10/04/91	3.6	2598	0.355 ± 0.013
0716+714	700210p	08/03/91	0.2	21043	0.802 ± 0.006
0735+178	700829p	27/10/02	0.3	6684	0.089 ± 0.004
0804+499	700846p	26/10/92	0.3	2999	0.053 ± 0.005
0836+710[1]	700493p	23/03/92	0.3	6993	0.742 ± 0.011
0836+710[2]	701061p	02/11/92	0.3	5026	0.378 ± 0.010
0851+202[1]	700219p	16/04/91	0.2	3622	0.273 ± 0.009
0851+202[2]	700426p	09/11/91	0.2	6785	0.606 ± 0.010
0851+202[3]	701391p	17/10/93	0.2	3285	0.641 ± 0.015
0906+430	700329p	13/11/91	0.2	23561	0.050 ± 0.002
0917+449	701398p	25/11/93	0.5	3367	0.201 ± 0.008
0954+556	701401p	07/11/93	0.2	4472	0.089 ± 0.005
0954+658	700042p	16/04/91	0.3	6772	0.052 ± 0.003

TABLE 2—*Continued*

Name[a]	ROR[b]	Start Time	Off–axis (arcmin)	exposure (seconds)	count rate (cts/sec)
1101+384[1]	700129p	04/05/93	0.2	4304	30.650 ± 0.084
1101+384[2]	700925p	04/06/93	0.2	9531	30.570 ± 0.058
1219+285	700223p	14/06/91	0.2	15223	0.224 ± 0.005
1226+023	700191p	14/12/91	0.2	6243	6.410 ± 0.033
1253−055	700305p	02/01/92	0.2	8513	0.578 ± 0.090
1510−089	700854p	16/08/92	0.0	5153	0.191 ± 0.007
1611+343	700842p	30/08/92	0.2	6804	0.122 ± 0.046
1633+382	700841p	28/08/92	0.3	5781	0.214 ± 0.007
1652+398	700130p	24/02/91	0.2	7649	6.950 ± 0.031
2005−489[1]	700488p	27/04/92	0.2	11487	2.780 ± 0.016
2005−489[2]	701057p	28/10/92	0.2	11462	1.704 ± 0.013
2155−304	700924p	16/11/92	0.4	1537	36.390 ± 0.158
2251+158[1]	700076p	26/11/91	0.1	6413	0.269 ± 0.007
2251+158[2]	700759p	26/05/92	0.1	8154	0.441 ± 0.008
2251+158[3]	900339p	15/12/92	0.1	22156	0.358 ± 0.004

[a]The source numbering is for reference to Table 2 reporting the spectral analysis results.

[b]Rosat observation number (ROR).

[c]for AO 0235+164 eight RORs are available, covering the period 21/07/1993–15/08/1993. The inspection of the light curve revealed a significant variability in terms of source count rate, so that we have NOT merged the full data set. Instead we have merged only the RORs having a source count rate at the same level, without including the two RORs: 701382p and 710383p. The detailed analysis of the full data set is reported in Madejski et al. (1996).

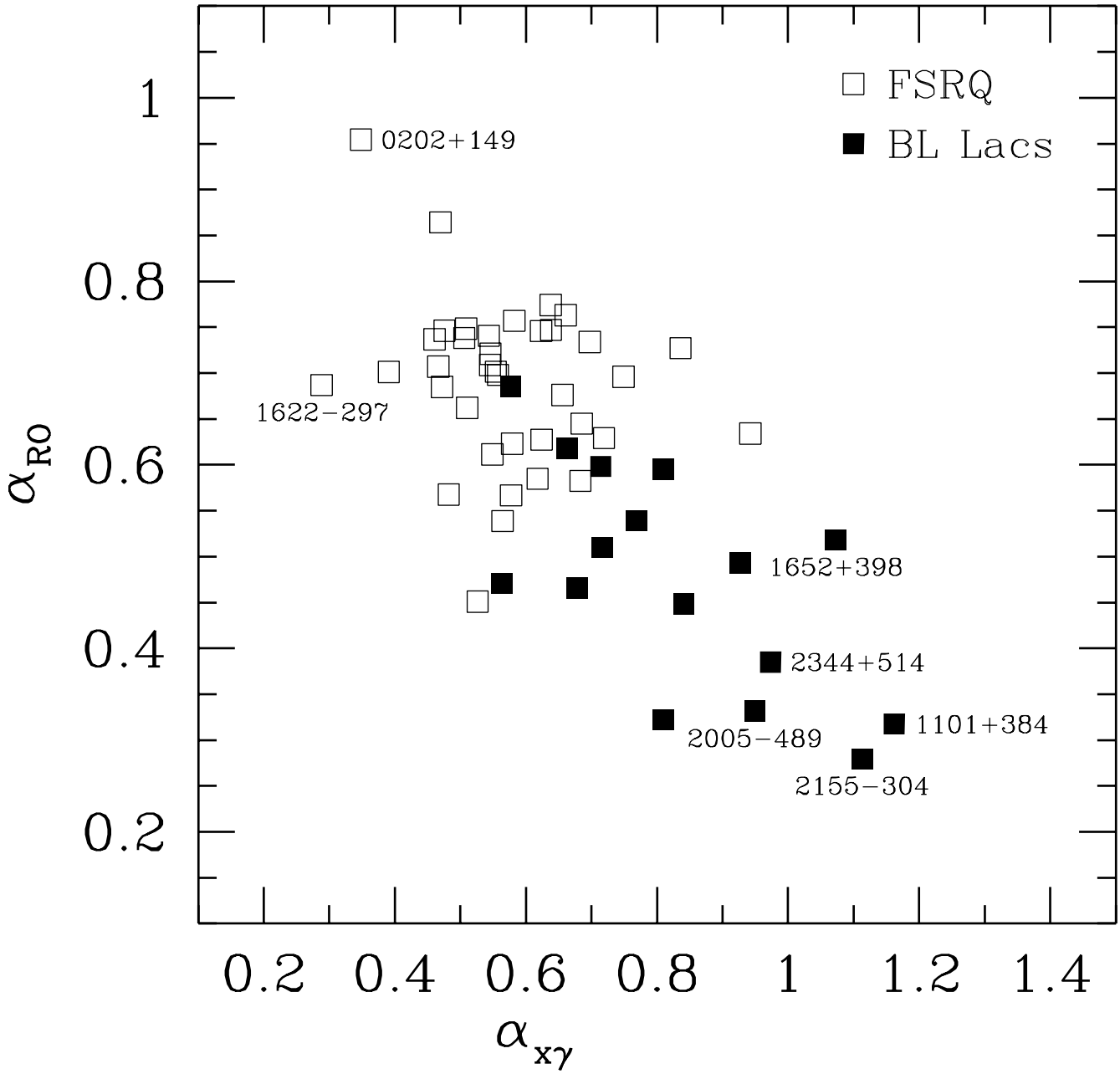
FSRQ
BL Lacs
0202+149
1622−297
1652+398
2344+514
1101+384
2005−489
2155−304
1
0.8
0.6
0.4
0.2
α_{RO}
0.2
0.4
0.6
0.8
1
1.2
1.4
$\alpha_{x\gamma}$

TABLE 3
SINGLE POWER LAW SPECTRAL FITS

Name	$N_{Hgal.}$[a]	α[b]	F_{1keV}[c]	χ^2/dof[d]	Free N_H[e]	α[b]	χ^2/dof[d]	Ref.
0202+149	5.89	$-0.32^{+0.54}_{-0.56}$	0.06	5.94/5	...	...	...	...
0208−512[1]	2.91	$1.08^{+0.14}_{-0.13}$	0.61	19.3/15	2.02 (1.02 − 3.27)	$0.79^{+0.43}_{-0.39}$	16.8/14	...
0208−512[2]	2.91	$1.11^{+0.12}_{-0.13}$	0.58	6.68/10	2.38 (1.13 − 3.90)	$0.93^{+0.54}_{-0.47}$	6.03/9	...
0208−512[3]	2.91	$1.10^{+0.12}_{-0.12}$	0.60	24.1/16	1.75 (0.72 − 3.06)	$0.75^{+0.42}_{-0.39}$	20.4/15	...
0208−512[4]	2.91	$0.88^{+0.12}_{-0.12}$	0.71	13.4/18	1.94 (0.77 − 3.38)	$0.58^{+0.47}_{-0.44}$	11.2/17	...
0208−512[5]	2.91	$0.98^{+0.11}_{-0.13}$	0.66	15.2/18	1.97 (0.87 − 3.35)	$0.67^{+0.47}_{-0.43}$	13.0/17	...
0208−512[6]	2.91	$0.95^{+0.11}_{-0.12}$	0.67	25.9/21	1.76 (0.91 − 2.77)	$0.57^{+0.36}_{-0.34}$	20.1/10	...
0208−512[7]	2.91	$1.08^{+0.12}_{-0.13}$	0.55	26.1/19	0.85 (0.58 − 1.95)	$0.36^{+0.43}_{-0.37}$	12.6/18	...
0208−512[8]	2.91	$1.01^{+0.10}_{-0.12}$	0.63	34.5/22	1.88 (0.93 − 3.05)	$0.66^{+0.41}_{-0.39}$	30.8/21	...
0208−512[9]	2.91	$1.20^{+0.10}_{-0.11}$	0.56	20.1/21	2.46 (1.43 − 3.68)	$1.05^{+0.42}_{-0.39}$	19.4/21	...
0208−512[10]	2.91	$1.04^{+0.09}_{-0.09}$	0.62	42.7/23	1.80 (0.98 − 2.77)	$0.68^{+0.34}_{-0.31}$	36.8/22	...
0208−512[11]	2.91	$0.99^{+0.15}_{-0.16}$	0.60	13.9/11	1.75 (0.50 − 3.41)	$0.60^{+0.58}_{-0.53}$	11.5/10	...
0208−512[12]	2.91	$0.98^{+0.16}_{-0.18}$	0.60	8.8/8	2.27 (0.76 − 4.29)	$0.78^{+0.62}_{-0.56}$	8.2/7	...
0219+428[1]	9.15	$1.49^{+0.04}_{-0.04}$	1.25	8.9/19	10.1 (8.9 − 11.5)	$1.60^{+0.17}_{-0.17}$	6.19/18	...
0235+164[1]	7.60	$0.51^{+0.13}_{-0.13}$	1.15	25.56/16	24.6 (12.4 − 41.3)	$1.59^{+0.97}_{-0.76}$	13.32/15	M96
0235+164[2]	7.60	$0.41^{+0.17}_{-0.18}$	0.41	17.58/12	26.12 (10.3 − 48.9)	$1.54^{+0.88}_{-0.97}$	10.01/11	M96
0521−365	3.37	$0.89^{+0.04}_{-0.05}$	2.12	14.76/22	3.83 (3.45 − 4.23)	$1.04^{+0.11}_{-0.11}$	10.02/21	P96
0528+134[1]	41.0	$0.75^{+0.51}_{-0.53}$	0.59	4.7/8	...	...	...	Z94
0528+134[2]	41.0	$0.45^{+0.35}_{-0.36}$	0.70	8.9/9	...	...	...	Z94
0537−441	2.91	$1.16^{+0.08}_{-0.09}$	0.81	21.1/14	2.94 (1.97 − 4.04)	$1.16^{+0.36}_{-0.33}$	21.1/13	T93,C95
0716+714	3.05	$1.76^{+0.02}_{-0.02}$	1.28	78.2/69	2.91 (2.69 − 3.14)	$1.71^{+0.09}_{-0.08}$	76.5/68	C94
0735+178	4.35	$1.25^{+0.16}_{-0.17}$	0.24	8.72/8	3.04 (1.64 − 4.28)	$0.89^{+0.50}_{-0.47}$	5.74/7	C95
0804+499	4.61	$0.56^{+0.33}_{-0.39}$	0.17	2.8/4	...	...	...	...
0836+710[1]	2.83	$0.42^{+0.05}_{-0.04}$	2.20	15.6/18	3.23 (2.74 − 3.75)	$0.52^{+0.14}_{-0.11}$	12.5/17	B94
0836+710[2]	2.83	$0.44^{+0.08}_{-0.08}$	1.11	27.8/18	3.60 (2.72 − 4.61)	$0.63^{+0.24}_{-0.24}$	24.3/17	B94
0851+202[1]	2.75	$1.14^{+0.09}_{-0.08}$	0.62	8.25/11	3.06 (2.11 − 4.14)	$1.25^{+0.37}_{-0.35}$	7.8/10	C95
0851+202[2]	2.75	$1.60^{+0.04}_{-0.04}$	1.00	24.0/29	2.29 (1.89 − 2.71)	$1.43^{+0.17}_{-0.16}$	18.6/28	...
0851+202[3]	2.75	$1.29^{+0.06}_{-0.05}$	1.30	16.0/20	2.68 (2.11 − 3.31)	$1.27^{+0.22}_{-0.21}$	15.9/19	...
0906+430	1.40	$0.57^{+0.10}_{-0.11}$	0.11	23.9/13	< 0.58	$0.01^{+0.28}_{-0.11}$	6.1/12	...
0917+449	1.50	$0.39^{+0.10}_{-0.09}$	0.47	20.3/14	2.82 (1.70 − 4.12)	$0.80^{+0.38}_{-0.36}$	13.7/13	...
0954+556	0.88	$1.17^{+0.14}_{-0.13}$	0.10	13.0/10	0.79 (0.09 − 1.89)	$1.13^{+0.52}_{-0.42}$	13.0/9	...
0954+658	3.71	$0.23^{+0.24}_{-0.26}$	0.17	5.53/7	7.19 (2.42 − 32.22)	$0.67^{+1.55}_{-0.74}$	3.6/6	C95
1101+384[1,f]	1.61	$1.95^{+0.03}_{-0.03}$	31.5	56.2/25	5.06 (3.57 − 6.95)	$2.23^{+0.15}_{-0.12}$	18.5/24	...
1101+384[2,f]	1.61	$1.82^{+0.02}_{-0.02}$	36.1	125.5/55	5.33 (4.23 − 6.57)	$2.10^{+0.09}_{-0.08}$	43.5/54	...
1219+285	1.95	$1.19^{+0.05}_{-0.05}$	0.41	22.86/19	2.25 (1.76 − 2.70)	$1.30^{+0.21}_{-0.20}$	21.22/18	...
1226+023	1.69	$0.95^{+0.01}_{-0.01}$	12.3	88.6/47	1.53 (1.42 − 1.64)	$0.89^{+0.05}_{-0.05}$	79.4/46	...
1253−055	2.22	$0.83^{+0.04}_{-0.03}$	1.34	27.8/36	2.40 (1.99 − 2.82)	$0.89^{+0.14}_{-0.14}$	27.0/35	...
1510−089	7.88	$0.90^{+0.16}_{-0.17}$	0.74	13.6/15	8.17 (5.82 − 12.76)	$0.93^{+0.42}_{-0.36}$	13.6/14	...

TABLE 3—*Continued*

Name	$N_{Hgal.}$[a]	α[b]	F_{1keV}[c]	χ^2/dof[d]	Free N_H[e]	α[b]	χ^2/dof[d]	Ref.
1611+343	1.44	$0.76^{+0.06}_{-0.05}$	0.24	15.4/12	0.87 (0.28 − 1.62)	$0.53^{+0.32}_{-0.30}$	12.6/11	···
1633+382	1.02	$0.53^{+0.08}_{-0.07}$	0.42	27.7/16	1.68 (0.91 − 2.58)	$0.78^{+0.32}_{-0.41}$	24.4/15	···
1652+398	1.73	$1.35^{+0.02}_{-0.02}$	10.1	299.0/110	2.37 (2.26 − 2.49)	$1.60^{+0.05}_{-0.04}$	117.1/109	C95
2005−489[1]	4.96	$2.21^{+0.02}_{-0.02}$	5.30	227.2/94	3.97 (3.79 − 4.15)	$1.89^{+0.07}_{-0.07}$	99.8/93	C95,S95
2005−489[2]	4.96	$2.39^{+0.02}_{-0.02}$	2.79	245.0/94	3.51 (3.29 − 3.73)	$1.89^{+0.08}_{-0.08}$	77.5/93	S95
2155−304	1.36	$1.38^{+0.01}_{-0.01}$	43.90	146.1/93	1.27 (1.19 − 1.36)	$1.34^{+0.04}_{-0.03}$	141.4/92	···
2251+158[1]	7.83	$0.46^{+0.13}_{-0.13}$	1.04	14.7/16	10.01 (6.78 − 16.98)	$0.65^{+0.45}_{-0.34}$	13.1/15	···
2251+158[2]	7.83	$0.50^{+0.08}_{-0.09}$	1.70	28.3/29	8.61 (7.06 − 10.96)	$0.57^{+0.21}_{-0.19}$	27.3/28	···
2251+158[3]	7.83	$0.72^{+0.06}_{-0.06}$	1.38	35.0/28	7.07 (6.28 − 8.02)	$0.65^{+0.12}_{-0.12}$	31.9/27	···

[a] Galactic column density (units of 10^{20} cm^{-2}). For 0235+164, 0521−365, 0735+178, 0851+202, 1611+343, 1641+399, 1652+398, 2251+158 the Galactic column densities are from Elvis et al. (1989). For 0537-441, 0716+714, 0836+710, 0906+430, 0954+556, 1633+382 from Murphy et al (1996). For 0851+202, 1101+384, 1226+023, 1510−089, 2155−304, 2251+158 from Lockman and Savage (1995). For the other objects the values are from Dickey & Lockman (1990).

[b]Energy spectral index.

[c]Flux at 1 keV (in μJy).

[d]Total χ^2 and degrees of freedom.

[e]Column density obtained from the X–ray spectral fits (units of 10^{20} cm^{-2}). For the weak sources only spectral fits with N_H fixed at the Galactic value are reported. Errors are quoted at 90% confidence intervals for one interesting parameter ($\chi^2_{min}+2.71$, column 3), and for two parameters ($\chi^2_{min}+4.61$, columns 6 and 7).

[f] Due to problems related with a gain shift the data were fitted only in the interval $0.5-2.2$ keV.

References.— (B94) Brunner et al. 1994; (C94) Cappi et al. 1994; (C95) Comastri, Molendi and Ghisellini 1995; (M96) Madejski et al. 1996; (P96) Pian et al. 1996; (S95) Sambruna et al. 1995; (T93) Treves et al. 1993; (Z94) Zhang et al. 1994

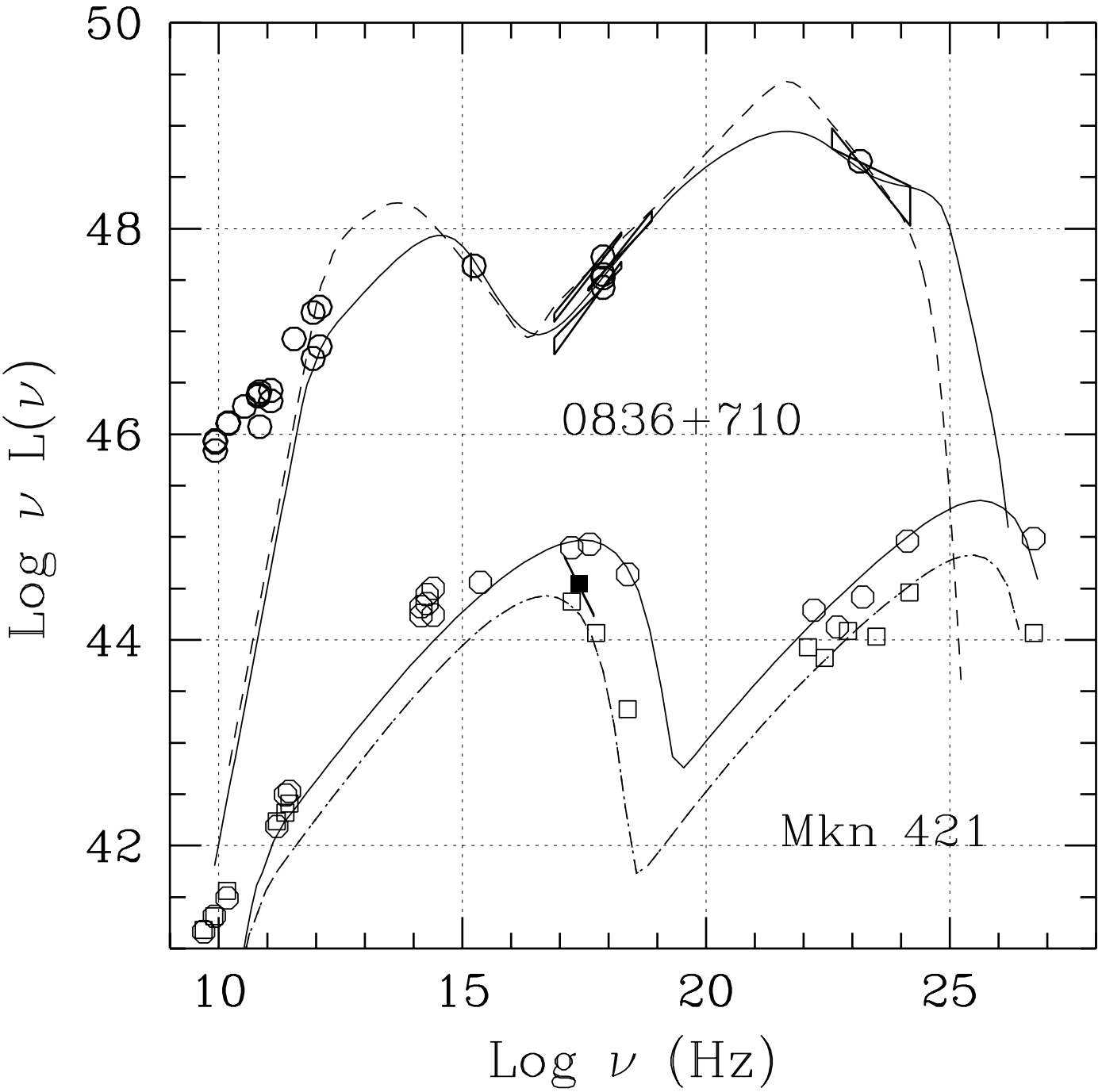
50
48
46
44
42
Log ν L(ν)
0836+710
Mkn 421
10
15
20
25
Log ν (Hz)

TABLE 1
SELECTED SAMPLE

IAU Name (1)	Other (2)	class (3)	z (4)	γ detection (σ)[a] (5)	VP[b] (6)	Ref. (7)	X
0202+149	4C 15.05	FSRQ	1.202	5.3	21.0	1st/ Lin96	
0208−512	PKS	FSRQ	1.003	21.5	10.0	Ber93/ Lin96	
0219+428	3C 66A	BL Lac	0.444	6.3	I+II	Din96	
0234+285	CTD 20	FSRQ	1.213	6.0	I+II	Din96	
0235+164	AO	BL Lac	0.940	13.0	21.0	Lin96	
0336−019	CTA 26	FSRQ	0.852	> 4	···	6161	
0420−014	PKS	FSRQ	0.915	6.7	21.0	Lin96	
0454−234	PKS	FSRQ	1.009	> 4	29.0	Tho93	
0454−463	PKS	FSRQ	0.858	> 5	6.0	vMon95	
0458−020	4C −2.19	FSRQ	2.286	4.4	29.0	2nd	
0506−612	PKS	FSRQ	1.093	>4	I+II	vMon95	
0521−365	PKS	FSRQ	0.055	>4	29.0	Lin95	
0528+134	OG 147	FSRQ	2.07	13.0	1.0	2nd	
0537−441	PKS	BL Lac	0.894	5.3	6.0	Lin96	
0716+714	S5	BL Lac	≥ 0.3	5.9	18.0	Lin95	
0735+178	PKS	BL Lac	≥ 0.424	4	I+II	2nd	
0804+499	OJ 508	FSRQ	1.433	6.0	I+II	Nol96	
0827+243	OJ 248	FSRQ	0.939	5.2	I+II	Nol96	
0829+046	OJ 049	BL Lac	0.18	4.1	I	2nd	
0836+710	4C 71.07	FSRQ	2.172	6.0	18.0+22.0	Tho93	
0851+202	OJ 287	BL Lac	0.306	4.0	···	Shr96	
0906+430	3C 216	FSRQ	0.670	> 4	4.0	Tho93	
0917+449	S4	FSRQ	2.18	6.5	I+II	Sre96/ 2nd	
0954+556	4C 55.17	FSRQ	0.901	4.2	I+II	Sre96	
0954+658	S4	BL Lac	0.368	5.7	227.0+228.0	Muk95	
1101+384	Mkn 421	BL Lac	0.031	8.5	I+II	Sre96/2nd	
1127−145	PKS	FSRQ	1.187	6.0	206.0	Sre96/ 2nd	
1156+295	4C 29.45	FSRQ	0.729	6.8	206.0	Sre96	
1219+285	ON 231	BL Lac	0.102	5.0	I+II	Sre96	
1222+216	4C 21.35	FSRQ	0.435	> 4	3.0+4.0	Sre96	
1226+023	3C 273	FSRQ	0.158	4.1	3.0	2nd	
1229−021	PKS	FSRQ	1.045	4.8	I+II	Sre96/ 2nd	
1253−055	3C 279	FSRQ	0.538	44.6	3.0	Sre96/2nd	
1317+520	4C 52.27	FSRQ	1.060	4.0	I+II	2nd	
1510−089	PKS	FSRQ	0.361	4.7	I+II	Sre96/ 2nd	
1604+159	4C 15.54	BL Lac	0.357	4.9	25.0	Sre96	
1606+106	4C 10.45	FSRQ	1.227	7.8	I	2nd	
1611+343	DA 406	FSRQ	1.404	7.9	II	2nd	
1622−297	PKS	FSRQ	0.815	> 25	421.0–423.5	Mat96	
1633+382	4C 38.41	FSRQ	1.814	17.3	9.2	Sre96/2nd	
1652+398	Mkn 501	BL Lac	0.055	8.4	···	Q96[c]	
1730−130	NRAO 530	FSRQ	0.902	5.7	I+II	Nol96	

TABLE 1—*Continued*

IAU Name (1)	Other (2)	class (3)	z (4)	γ detection (σ)[a] (5)	VP[b] (6)	Ref. (7)	X–ray class (8)
1739+522	4C 51.37	FSRQ	1.375	7.2	I+II	Nol96	RASS
1741−038	OT 68	FSRQ	1.054	> 5	I+II	vMon95	RASS
1933−400	PKS	FSRQ	0.966	6.6	I+II	Din96	RASS
2005−489	PKS	BL Lac	0.071	3.7	I	Lin96	pointed
2032+107	PKS	BL Lac	0.610	6.2	I+II	Din96	—
2052−474	PKS	FSRQ	1.489	4.2	I	2nd	RASS
2155−304	PKS	BL Lac	0.117	~ 4	404.0	Ves95	pointed
2230+114	CTA 102	FSRQ	1.037	7.0	19.0	2nd	RASS
2251+158	3C 454.3	FSRQ	0.859	13.4	19.0	Har93/Lin96	pointed
2344+514	PKS	BLLac	0.044	~ 5	$\cdots$	Feg96[c]	—
2356+196	PKS	FSRQ	1.066	4.6	42.0	Lin96	RASS

[a]Significance of the γ–ray detection. For EGRET data this corresponds to the standard estimator $\sqrt{TS}$

[b]Viewing period number, or if "I", "II", "I+II", data averaged over the whole phase one, phase two or p
plus two respectively

[c]This source has been detected only by Whipple Observatory above 300 GeV

References.— (tw) = this work, see Table 2; (1st) = Fichtel et al. 1994 (First EGRET sources catalo
= Thompson et al. 1995 (Second EGRET sources catalog); (6161) = IAU circular 6161; (Ber93) = Bert
1993; (Br94) = Brinkmann et al. 1994; (Br95) = Brinkmann et al. 1995; (Din96) = Dingus et al. 1996; (
Fegan 1996; (Gi94) = Giommi et al. 1994; (Har93) = Hartman et al. 1993; (Lin95) = Lin et al. 1995; (
Lin et al. 1996; (Mat96) = Mattox et al. 1996; (Muk95) = Mukherjee et al. 1995; (Nol96) = Nolan et
(Per96) = Perlman et al. 1996; (Q96) = Quinn et al. 1996; (Shr96) = Shrader et al. 1996; (Sre96) = S
et al. 1996; (Tho93) = Thompson et al. 1993; (Ves95) = Verstrand et al. 1995; (vMon95) = von Monti
1995; (Wi94) = Wilkes et al. 1994; (WW90) = Worral & Wilkes 1990

TABLE 4
Double Power–Law Spectral Fits

Name	$N_H^{gal.}$ [a]	α_1 [b]	E_{break} [c]	F_{1keV} [d]	α_2 [e]	F_{1keV} [f]	χ^2/dof [g]
0235+164[1]	7.60	< 0.21	0.86	...	$0.99^{+0.57}_{-0.31}$	1.29	12.8/13
0235+164[2]	7.60	< -0.1	0.68	...	$0.77^{+0.33}_{-0.28}$	0.44	8.2/9
0906+430[h]	1.40	$6.57^{+0.11}_{-0.14}$	...	$6.2 \cdot 10^{-6}$	0.10	0.10	5.8/12
1101+384[1]	1.61	$1.69^{+0.16}_{-0.45}$	0.85	...	$2.15^{+0.29}_{-0.11}$	32.5	17.2/23
1101+384[2]	1.61	$1.44^{+0.20}_{-0.78}$	0.75	...	$1.95^{+0.08}_{-0.05}$	36.7	49.4/53
1226+023[i]	1.69	$1.37^{+0.16}_{-0.14}$	...	4.50	0.54	7.66	61.3/46
1652+398	1.73	$0.43^{+0.31}_{-0.31}$	0.31	...	$1.57^{+0.05}_{-0.05}$	9.85	122.1/108
2005−489[1]	4.96	$4.69^{+1.46}_{-1.02}$	...	0.066	$1.88^{+0.06}_{-0.12}$	5.32	97.8/92
2005−489[2]	4.96	$4.85^{+1.32}_{-1.11}$	...	0.049	$1.86^{+0.10}_{-0.21}$	2.84	72.1/93

[a]Galactic column density (units of 10^{20} cm^{-2}).

[b]Energy spectral index of the soft component.

[c]Break energy in keV for the sources fitted with a broken power law model.

[d]Flux at 1 keV (in μJy) of the soft component, for the sources fitted with a double power law model.

[e]Energy spectral index of the hard component.

[f]Flux at 1 keV (in μJy) of the hard component.

[g]Total χ^2 and degrees of freedom.

[h]The adopted value for the hard X–ray spectral index has been fixed at the best fit value found in the fit. Due to the poor statistical quality of the PSPC spectrum the errors on the soft component have been computed freezing all the other fit parameters.

[i]The hard slope has been fixed at the best fitting value of Ginga (2–10 keV; Lawson & Turner 1996), which is consistent with our fit.

TABLE 5a

MULTIFREQUENCY DATA: FLAT SPECTRUM RADIO QUASARS

IAU Name	z	F_{5GHz} (Jy)	Ref.	$F_{5500\mathring{A}}$ (mJy)	Ref.	F_{1keV} (μJy)	α_X	Ref.	F_γ[a]	α_γ
(1)	(2)	(3)	(4)	(5)	(6)	(7)	(8)	(9)	(10)	(11
0202+149	1.202	2.40	Pe82	0.017	IT90	0.06	-0.32 ± 0.55	tw	2.6	1.5 ±
0208−512	1.003	3.26	K81	0.64	IT88	0.61	1.04 ± 0.04	tw	9.1	0.69 ±
0234+285	1.213	2.36	Pe82	0.186	K81	0.09	···	Br95	1.51	1.7 ±
0336−019	0.852	2.84	K81	0.45	K81	0.10	···	Br94	∼ 10.0	··
0420−014	0.915	3.72	Pe82	0.34	WP85	0.44	···	Br94	4.96	0.9 ±
0454−234	1.009	2.2	Le85	0.91	IT88	0.09	···	Wi94	1.4	··
0454−463	0.858	2.97	K81	0.246	K81	0.16	···	Br94	2.9	0.9 ±
0458−020	2.286	2.04	Le85	0.17	K81	0.10	···	Wi94	3.11	··
0506−612	1.093	2.1	K81	0.68	IT90	0.28	···	Br94	0.6	··
0521−365	0.055	9.7	K81	2.38	Pi94	2.12	0.89 ± 0.05	tw	1.8	1.16 ±
0528+134	2.07	4.3	Pe82	0.308	WP85	0.65	0.54 ± 0.29	tw	8.39	1.6 ±
0804+499	1.433	2.05	K81	0.39	K81	0.17	0.56 ± 0.36	tw	1.49	1.72 ±
0827+243	0.939	0.67	Be91	0.391	Ma93	0.34	···	Br95	2.46	1.21 ±
0836+710	2.172	2.67	Pe82	0.98	K81	1.60	0.42 ± 0.04	tw	2.1	1.41 ±
0906+430	0.670	1.80	K81	0.383	Ma86	0.11	0.01 ± 0.28	tw	3.2	··
0917+449	2.18	1.03	GC91	0.065	K81	0.47	0.39 ± 0.10	tw	1.19	0.98 ±
0954+556	0.901	2.28	K81	0.374	K81	0.10	1.17 ± 0.14	tw	0.61	0.63 ±
1127−145	1.187	7.46	K81	0.652	K81	0.34	···	Br94	9.27	1.15 ±
1156+295	0.729	1.65	Ge94	5.1	Gh86	0.8	0.86 ± 0.15[b]	Br95	19.22	1.21 ±
1222+216	0.435	0.81	GC91	0.39	HB93	0.41	···	Br95	2.34	1.50 ±
1226+023	0.158	44.6	K81	24.6	K81	12.30	0.89 ± 0.05	tw	2.38	1.4 ±
1229−021	1.045	1.1	K81	0.744	K81	0.08	···	Wi94	1.02	1.92 ±
1253−055	0.538	16.6	K81	15.10	Shr94	1.34	0.83 ± 0.04	tw	28.68	0.89 ±
1317+520	1.060	0.66	GC91	0.62	HB93	0.06	···	Br95	0.77	··
1510−089	0.361	3.35	K81	1.39	WP85	0.74	0.90 ± 0.16	tw	2.30	1.51 ±
1606+106	1.227	1.78	K81	0.155	K81	0.08	···	Br95	3.35	1.2 ±
1611+343	1.404	3.08	Ge94	0.39	K81	0.24	0.76 ± 0.06	tw	4.79	1.0 ±
1622−297[c]	0.815	1.92	K81	0.367	Mat97	0.08	···	Mat97	27.0[c]	1.2 ±

TABLE 5A—*Continued*

IAU Name	z	F_{5GHz} (Jy)	Ref.	$F_{5500\mathring{A}}$ (mJy)	Ref.	F_{1keV} (μJy)	α_X	Ref.	F_γ[a]	α_γ
(1)	(2)	(3)	(4)	(5)	(6)	(7)	(8)	(9)	(10)	(11)
1633+382	1.814	4.08	WP85	0.246	WP85	0.42	0.53 ± 0.08	tw	10.51	1.03 ± 0.0
1730−130	0.902	6.9	Gr94	0.52	RS85	0.63	···	Br94	2.18	1.39 ± 0.2
1739+522	1.375	1.98	K81	0.155	K81	0.16	···	Br95	2.38	1.23 ± 0.3
1741−038	1.054	3.72	K81	0.486	K81	0.61	···	Br94	3.4	2.0 ± 0.4
1933−400	0.966	1.48	K81	0.13	K81	0.30	···	Br94	1.3	1.4 ± 0.2
2052−474	1.489	2.52	K81	0.296	K81	0.23	···	Br94	2.22	1.4 ± 0.4
2230+114	1.037	4.1	Pe82	0.47	K81	0.29	···	Br94	2.69	1.6 ± 0.2
2251+158	0.859	23.3	WP85	1.58	K81	1.37	0.62 ± 0.04	tw	8.0	1.18 ± 0.0
2356+196	1.066	0.70	Be91	0.246	Pr85	0.28	···	Br95	3.02	···

TABLE 5B

MULTIFREQUENCY DATA: BL LAC OBJECTS

IAU Name	z	F_{5GHz} (Jy)	Ref.	$F_{5500\mathring{A}}$ (mJy)	Ref.	F_{1keV} (μJy)	α_X	Ref.	F_γ[a]	α_γ
(1)	(2)	(3)	(4)	(5)	(6)	(7)	(8)	(9)	(10)	(11)
0219+428	0.444	1.04	VV93	3.96	VV93	1.25	1.49 ± 0.04	tw	1.63	$0.9 \pm$
0235+164	0.940	2.85	St91	6.6	Gh86	0.78	1.57 ± 0.86	tw	8.25	$0.90 \pm$
0537−441	0.894	4.00	St91	2.05	Tr93	0.81	1.16 ± 0.09	tw	3.64	$1.0 \pm$
0716+714	≥ 0.3	1.12	K81	20.5	Bo90	1.28	1.76 ± 0.02	tw	2.0	$1.04 \pm$
0735+178	≥ 0.424	3.65	Ge94	6.9	Gh86	0.24	1.25 ± 0.17	tw	1.29	..
0829+046	0.18	1.65	Ge94	1.4	Gh86	1.07	...	WW90	1.9	..
0851+202	0.306	2.7	K81	4.0	Gh86	0.97	1.45 ± 0.18	tw	2.9	..
0954+658	0.368	1.46	K81	0.82	PR88	0.17	0.23 ± 0.25	tw	1.2	$0.85 \pm$
1101+384	0.031	0.73	Ge94	17.8	Gh86	33.8	2.14 ± 0.07	tw	1.43	$0.58 \pm$
1219+285	0.102	0.97	GC91	2.9	Gh86	0.41	1.19 ± 0.05	tw	0.58	$0.27 \pm$
1604+159	0.357	0.50	Le85	0.13	Le85	0.17	...	Gi94	3.98	$0.99 \pm$
1652+398	0.055	1.42	K81	3.3	Gh86	10.1	1.60 ± 0.05	tw	0.81[d]	..
2005−489	0.071	1.5	Gh86	30.0	Gh86	4.04	1.89 ± 0.05	tw	1.38	..
2032+107	0.601	0.77	WB92	2.05	Gi94	0.10	...	Gi94	1.53	$1.5 \pm$
2155−304	0.117	0.27	Le85	21.33	VV93	43.90	1.38 ± 0.01	tw	2.73	$0.71 \pm$
2344+514	0.044	0.215	Per96	2.366	Per96	3.22	...	Per96	0.62[d]	..

[a]γ–ray flux measured by EGRET above 100 MeV, except that for 1652+398 and 2344+514 (see note (d)). photons/cm^2/sec

[b]The spectral index is by Ginga, 2−10 keV, Lawson & Turner 1996

[c]For 1622−297 the adopted γ–ray flux is not the peak value observed during the June–July 1995 flare reported 1997, i.e. 170 $\times 10^{-7}$ photons/cm^2/sec. We have chosen the flux value measured shortly before and after the sho value. We think it is more homogeneous with all the other sources fluxes because it is very unlikely to observe such

[d]γ–ray flux detected by Whipple above 300 GeV, units are 10^{-11} photons/cm^2/sec

REFERENCES.— (tw) = this work, see Table 2; (1st) = Fichtel et al. 1994 (First EGRET source catalog); (2nd) = 1995 (Second EGRET source catalog); (6161) = IAU circular 6161; (Ber93) = Bertsch et al. 1993; (Be91) = Be (Bo90) = Boznyan et al. 1990; (Br94) = Brinkmann et al. 1994; (Br95) = Brinkmann et al. 1995; (Din96) = Di (Feg96) = Fegan 1996; (GC91) = Gregory & Condon 1991; (Ge94) = Gear et al. 1994; (Gh86) = Ghisellini et al Giommi et al. 1994; (Gr94) = Griffith et al 1994; (Har93) = Hartman et al. 1993; (HB93) = Hewitt & Burbidg Impey & Tapia 1988; (IT90) = Impey & Tapia 1990; (K81) = Kuhr et al. 1981; (Le85) = Ledden & O'Dell 1985; al. 1995; (Lin96) = Lin et al. 1996; (Ma86) = Maraschi et al. 1986; (Ma93) = Maoz et al. 1993; (Mat97) = Ma (Muk95) = Mukherjee et al. 1995; (Nol96) = Nolan et al. 1996; (Pe82) = Perley 1982; (Per96) = Perlman et al Preston et al. 1985; (PR88) = Pearson & Readhead, 1988; (Pi94) = Pian et al. 1994; (Q96) = Quinn et al. 1996; (Seaquist 1985; (Shr94) = Shrader et al. 1994; (Shr96) = Shrader et al. 1996; (Sre96) = Sreekumar et al. 1996; (St9 1991; (Tho93) = Thompson et al. 1993; (Tr93) = Treves et al. 1993; (Ves95) = Vestrand et al. 1995; (vMon95) = al. 1995; (VV93) = Veron & Veron 1993; (Wi94) = Wilkes et al. 1994; (WB92) = White & Becker 1992; (WP85) = 1985; (WW90) = Worral & Wilkes 1990

TABLE 6
Model Fit Parameters

Parameter		Mkn 421		0836+710	
		High State[a]	Low State[a]	SSC	EC
size of blob	R (cm)	$1 \cdot 10^{16}$	$1 \cdot 10^{16}$	$5 \cdot 10^{16}$	$7 \cdot 10^{16}$
beaming factor	δ	11	11	19	19
injection slope	s	1.7	1.7	3.7	3.1
minimum electron injected γ	γ_{min}	1	1	$4 \cdot 10^3$	150
maximum electron injected γ	γ_{max}	$8 \cdot 10^5$	$3.3 \cdot 10^5$	$1 \cdot 10^5$	$1 \cdot 10^4$
injected compactness (intrinsic)	ℓ_{inj}	$6 \cdot 10^{-3}$	$3 \cdot 10^{-3}$	0.3	0.4
BLR compactness, seen by blob	ℓ'_{BLR}	0	0	0	6
magnetic field	B (Gauss)	0.16	0.16	0.36	10.3

[a]The spectral distributions for both states have been "fitted" only with SSC model